Al-Mustansiriyah Journal of Science
ISSN: 1814-635X (print), ISSN:2521-3520 (online) Volume 32, Issue 3, 2021 DOI: http://doi.org/10.23851/mjs.v32i3.944

Research Article **Open Access**

Optical and Electrical Conductivity of SnO:Cu Nanoparticles

Mohammed J. Mohammed Ali

Department of Physics College of Science, Mustansiriyah University, Baghdad, IRAQ

Author email: mohammedjassim@uomustansiriyah.edu.iq

ArticleInfo

Received
13/01/2021

Accepted
04/02/2021

Published
20/06/2021

ABSTRACT

This study included a different weight ratio of copper (2, 4, 6, 8) wt% as a dopant, with tin oxide SnO_2 deposits on glass substrate by RF reactive magnetron sputter. The structural properties show polycrystalline pattern nature for all deposit samples with dominated reflection (110). The electrical conductivity increased to 1×130^{10} S^{-1} and the optical conductivity to 35×10^{16} S^{-1}. The energy gap decreased to 3.60 eV when the rate of deformation was 8wt%, due to the increase in the crystallite size to 24.5 nm with the improvement of crystallization. While the surface measurements showed an increase in the surface roughness to 50 nm when the rate of deformation at 8wt%.

KEYWORDS: Optical conductivity; Electrical Conductivity; RF sputters; Roughness; Line histogram.

الخلاصة

تضمنت هذه الدراسة التشويب بنسبة وزن مختلفة من النحاس (2 ، 4 ، 6 ، 8) مع ترسيب أكسيد القصدير SnO_2 على الركيزة الزجاجية بواسطة الترسيب بالرش المغنطي التفاعلي RF. تُظهر الخصائص الهيكلية طبيعة نمط متعدد البلورات لجميع العينات مع الانعكاس المسيطر (110). زادت الموصلية الكهربائية إلى 1×130^{10} S^{-1} والموصلية الضوئية إلى 35×10^{16} S^{-1}. انخفضت فجوة الطاقة إلى 3.60 فولت عند معدل التشويب 8٪ ، نتيجة زيادة حجم البلورة إلى 24.5 نانومتر مع تحسن التبلور. بينما أظهرت قياسات السطح زيادة في خشونة السطح إلى 50 نانومتر عند معدل التشويب 8٪.

INTRODUCTION

The thin-film and nanotechnology are the most important techniques that contributed to the enhancement and development of semiconductor materials applications [1][2]. Even in the balance of micro composition [3] and transparent conductive oxides (Transparent conductors) [4][5]. In addition, the oxide SnO_2 material has three advantages; a high conductivity, low resistivity, and high optical transmittance [6]. Where it all depends on the conditions of preparing these materials, and there is the possibility of free electrons in the conduction band, despite the large energy gap of these membranes. There are several preparing methods such as the R.F Sputtering [7], D.C Magnetron Sputtering [8], Electron Beam Evaporation [9], Evaporation Ion-Beam [10], Sol-Gel [11], Modified Successive Ionic Layer Adsorption [12], Vapor Deposition Chemical [13], Pulsed Laser [14], Thermal Evaporation [15] and Chemical spray pyrolysis [16]. Tin dioxide is a semiconductor with a large energy gap [17][18], it is a white color, material, and the crystalline structure of tin dioxide is a crystalline quaternary structure [19]. Recently, the researchers have tended to pay attention to SnO_2 film due to this material may be a part of many applications, such as used in optoelectronic devices, and indirect energy transfer devices [20][21].

Mani Facier *et. al.* Studied SnO_2 films prepared using two methods of vacuum thermal evaporation and chemical decomposition. They concluded that the edge of the absorption (2.4eV) by means of thermal evaporation. In the pyrolysis method, the absorption edge value (3.7eV) and the prepared crystalline membranes with an energy gap of is 3.5 eV for permissible direct transmission [22].

Sundaram & Bhagavat studied the optical absorption of the (SnO_2) films prepared by the CVD method. They concluded that the edge of absorption is at the energy (3.7eV), and the permissible direct/indirect energy gap was (3.95eV) and (3.27 eV), respectively [23]. In 2010 Huang et al., prepared pure tin dioxide films that

Copyright © 2021 *Al-Mustansiriyah Journal of Science*. This work is licensed under a Creative Commons Attribution Noncommercial 4.0 International License.

have been tainted with tungsten (SnO_2: W) with weights of distortion (0, 2, 3%), in a pulsed plasma precipitation method (PPDM) on quartz bases. The optical energy gap increased from 4.05eV to 4.22eV with increased distortion rates [24].

Moreover, Copper oxide is an important semiconductor material [25], and the concentration of free electrons in tin dioxide is (10^{16} cm^{-3}) [26]. Also, it is neither soluble in water nor in the bases and can be obtained from copper oxidation; and it is characterized by a mono-inclination crystal structure (p-type) meaning that the carriers of the majority are gaps [27]. Copper oxide has a relatively large energy gap and a high absorption coefficient in the visible area. Particularly, it is used in solar photothermal cells applications, as it requires high efficiency absorption and a range of good stability as well as high absorbency in the visible wavelength range [28].

The improvement in crystallization led to a decrease in the values of the energy gap (Eg). Therefore, this work aims to study the structural and optical properties resulting from tin oxide deformation at different proportions of copper; to determine the appropriate application of the semiconductor created.

MATERIALS AND METHODS

Tin oxide nanoparticles as a powder target composed with purity 99.998 and copper oxide nano partial 99.99 purity used as a dopant (2, 4, 6 and 8) wt%. Where deposited on a glass substrate by radio frequencies sputter down at frequency 13.56 MHz (TORR INTERNATIONAL, INC.CRC600). The RF power kept at a constant value 100 watt for all deposited films. Magnetic field used to maximize the deposition rate. The vertical distance between the target and the substrate is fixed to 10 cm. Substrate holder rotated with constants rate 5 Cyc/Min. Deposition rate was 0.1- 0.2 Å/sec and thickness 100 nm controlled by a crystal sensor (SQM-160). The chamber was evacuated to a pressure of under 3.82×10^{-5} torr before sputtering deposition. Argon gas penetrates to the chamber with a gas mass flue controller (Ailcat scientific), Sputtering was performed at a gas pressure approximately 5.62×10^{-2} Torr. As a film's characterization, the crystal structure of deposit films was identified and investigated by X-ray diffraction. by (shimadzo 6-2006, with cukα radiation having wavelength λ=0.15406 nm) technique. Optical properties investigated by *(Cary 100 conc UV-Visible spectroscopy).*

RESULTS AND DISCUSSION

Figure (1-a) displays the X-ray diffraction of the pure and copper doped tin oxide at a different weight ratio (2, 4, 6, 8) wt% and notes from the figure that all the membranes are poly-crystalline pattern. The prevailing reflection is the (110) plane at the angle $2\theta = 29.96^{o}$, with the number of secondary reflections in (101), (200), and (211) that associated with the angles $2\theta = 34.37^{o}$, 38.10^{o}, 51.58^{o} respectively. It is indicated with the international card JCPOS No. 41-1445 [29]. From figure (1-a), we have shown that the intensity of the dominant reflection (110) increases with an increased weight ratio for copper dopants.

The dominant reflection samples, figure (1-b) show up a magnified and groped image, as can be seen in which full width at half maximum (FWHM) is changed with the increased dopant. Either the figures (1-c and d) It is a magnified image (zoom-in) of secondary reflections (101), (200) as noted, from which the intensity of reflection changed with the increased doping of Cu.

As can be seen from figure (2-a) the crystallite size fluctuates between decreases and increases to 24.32 nm with the height weight ratio of Cu dopant. This is the result of the small size of copper ions Cu^{+2}= 58 Å Compared to SnO^{+4} ions = 71Å, which take interstitial locations. Thus decreases from lattice constant, thus for Cu up to 4 wt% adding Cu to (6 and 8) wt% leads to increase the crystalline size due to copper ions beginning to fill substation locations, the reason for the crystal size increases.

Also, figure (2-c, b) shows that the microstrain and dislocation density decreases with an increase in doping for ratios (2 and 4) wt% and increases for ratios (6 and 8) wt%. Due to the improving crystallization reduces crystal defects, micro-strain, and dislocation density. The estimate of the crystallite size, micro-strain and dislocation density were calculated by using the equations (1,2,3) and listed in Table (1), measured and calculated structural parameters [30].

$$D = \frac{k\lambda}{\beta \cos\theta} \quad (1)$$

Where λ =1.5405 Å, is the wavelength of the used X-ray, k = 0.9 is the geometrical constant, β is the FWHM in rad, and θ is the reflection angle.

$$\varepsilon = \frac{\beta \cos\theta}{4} \quad (2)$$

$$\delta = \frac{1}{D^2} \quad (3)$$

Table 1. Measured and calculated structural parameters of SnO :Cu

Samples (Wt%)	(hkl) Plane	2Θ [°]	FWHM [°]	(D) (nm)	Microstrian $\times 10^{-4}$(line^2.m^{-1})	Dislocation density $\times 10^{15}$(line.m^{-2})	Lattice constant (Å)	
							a	b
0	(110)	29.96	0.39	20.58	2.36	1.64	4.691	3.201
2	(110)	29.96	0.41	19.57	2.61	1.73	4.684	3.194
4	(110)	29.96	0.42	19.11	2.74	1.77	4.633	3.190
6	(110)	29.96	0.34	23.60	1.79	1.43	4.661	3.199
8	(110)	29.96	0.33	24.32	1.69	1.39	4.689	3.202

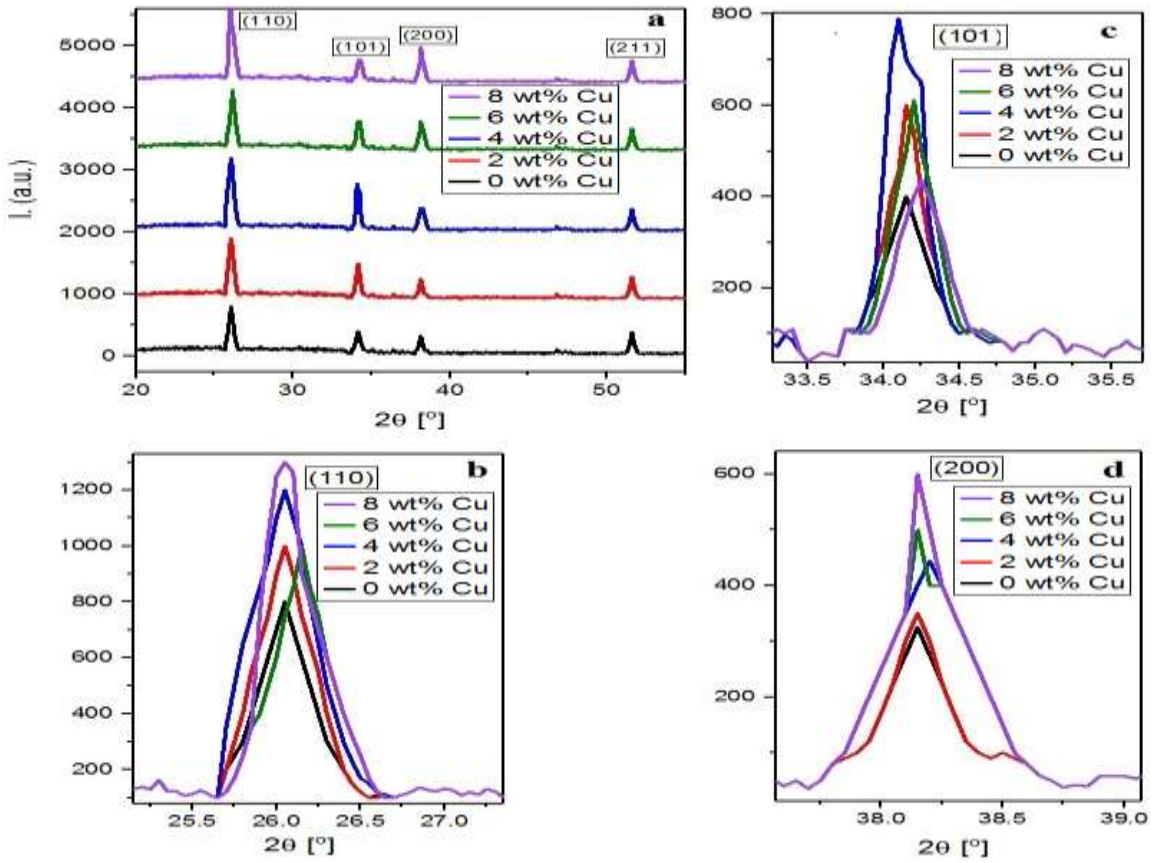

Figure 1. (a) X-ray diffraction pattern for pure and copper doped tin oxide, (b) dominates reflection, (c and d) secondary reflection.

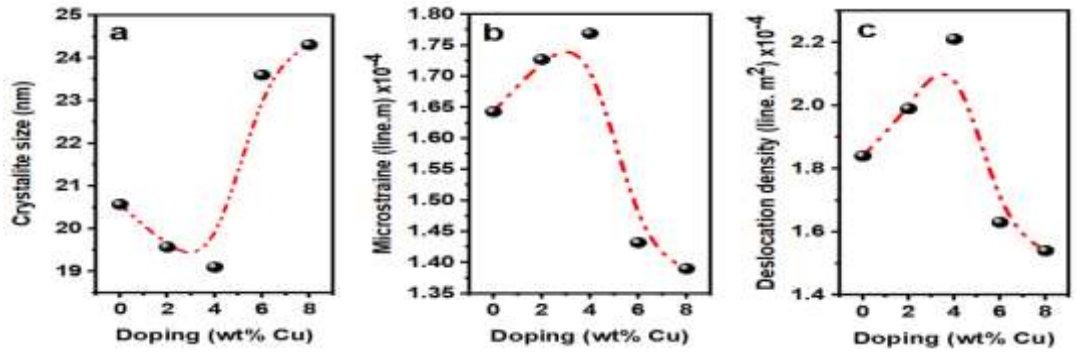

Figure 2. (a) Crystallite size (b) Microstrain (c) Dislocation density.

Copyright © 2021 *Al-Mustansiriyah Journal of Science*. This work is licensed under a Creative Commons Attribution Noncommercial 4.0 International License.

Figure (3- a and b) explain a 3D image of 0 wt% Cu SnO_2 deposited by RF magnetron sputter. The 2D image stands out in figure (3-c), and figure (3-d) shows the magnified image (zoom-in) to the surface. Figure (3-e) represents a graph of the X-axis when converting the image to data values, to get an accurate description of figures resulting from the dopant of thin film SnO_2 by Cu. For pure (SnO_2) thin films, figure (3-e) spotted the width of the formed peaks within 30 nm, with a height (20-50) nm, and average particle size within (40-60) nm.

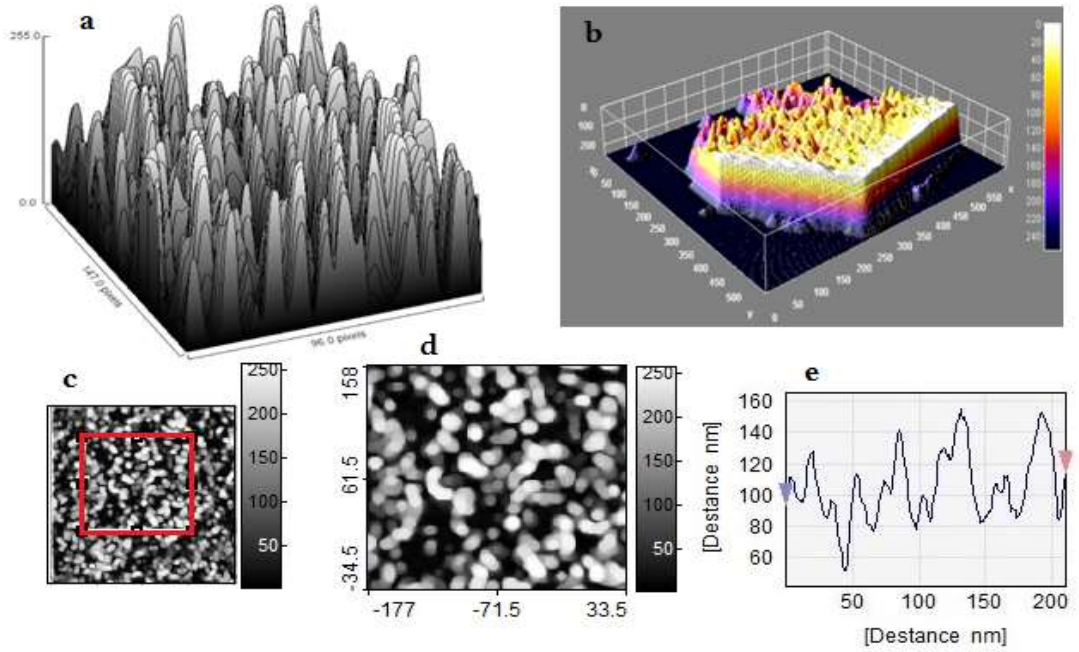

Figure 3. (a and b) Represent a 3D image of SnO_2 thin films doped with 0 wt% of Cu, (c) 2D image, (d) a magnified image (zoom-in) of the surface and (e) line, histogram as x and y graph.

Figure (4- a and b), stated the 3D image of 2 wt% Cu SnO_2 deposited by RF magnetron sputter, figure (4-c) represent a 2D image, figure (4-d) it is a magnified image (zoom-in) of surface, to make more accurate measurements as shown in figure (4-e). A two-dimensional image has been converted into values that can be plotted on two axes X-axis and Y-axis. Further, growing peaks have become more uniform and have a conical shape, which are nanostructures with a height up to 30 nm and a base width of around 50 nm.

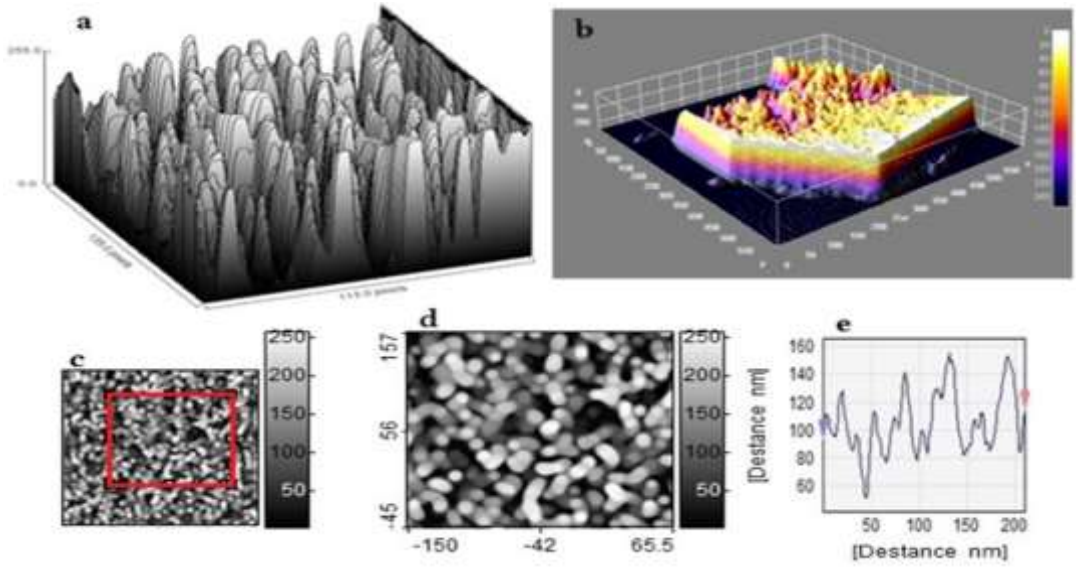

Figure 4. (a and b) Represent a 3D image of SnO_2 thin films doped with 2 wt% of Cu, (c) 2D image, (d) a magnified image (zoom-in) of the surface and (e) line, histogram as x and y graph.

Figure (5- a and b) illustrated, 3D image of 4 wt% Cu SnO_2 deposited by RF magnetron sputter, Figure (5-c) represent the 2D image, It is noted that the surface became more intense in the number of developing peaks and the white area increasing, which represents a height of about 200 nm. In addition, the decline of the black area representing the height of 50 nm, Figure (5-e) represents the process of converting the X-axis, which is chosen through a program Spip - software, which it is observed that the height of cone nano scale forms increases to 80-100 nm.

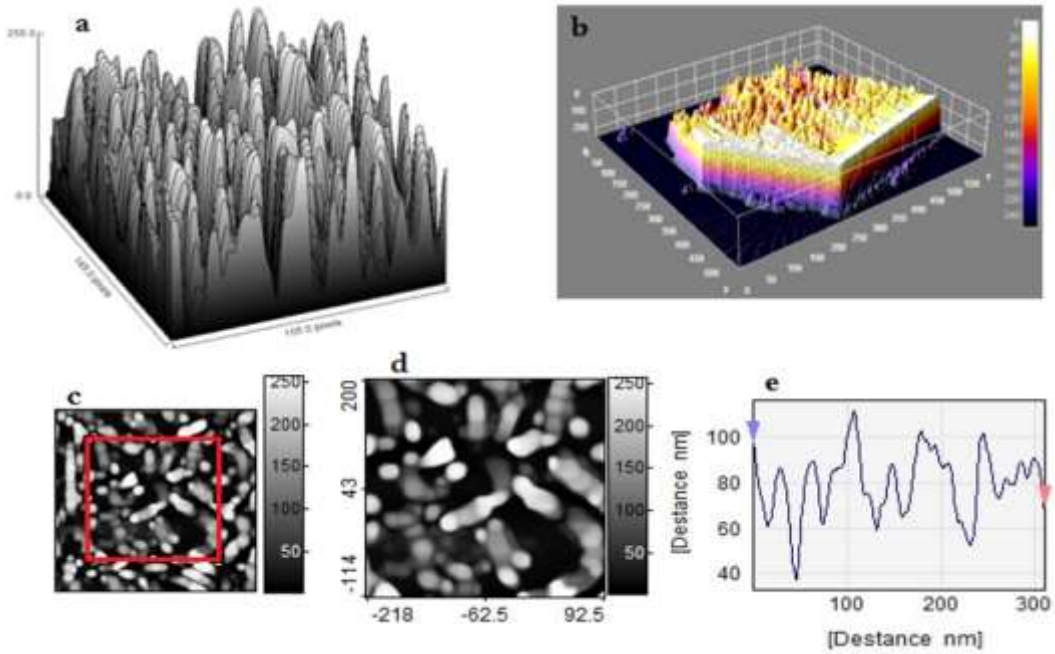

Figure 5. (a and b) Represent a 3D image of SnO_2 thin films doped with 4 wt% of Cu, (c) 2D image, (d) a magnified image (zoom-in) of the surface and (e) line, histogram as x and y graph**.**

In the figure 6, (a and b) can show the Cu SnO_2 deposited by RF magnetron sputter at 6 wt% has uniformly distributed particles with homogeneity. From the 2D image, the spherical shaped particles covered all the surface film deposited on the glass substrate. In addition, Figure (6-d and e) proves that the width of cones has become wider at its bases and less elevated.

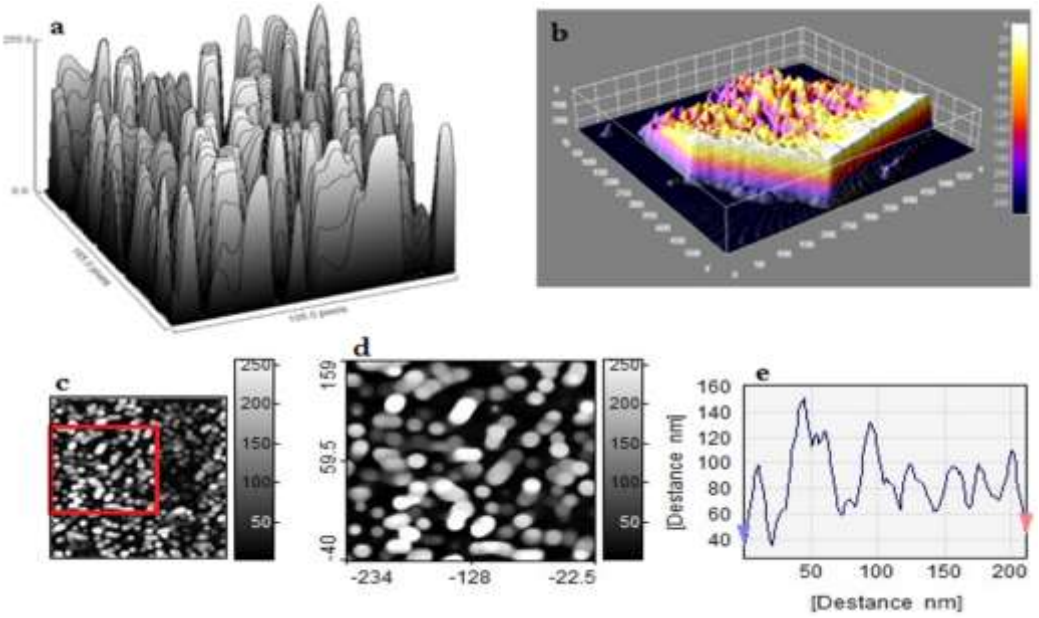

Figure 6. Illustrated (a and b) a 3D image of SnO_2 thin films doped with 6 wt% of Cu, (c) 2D image, (d) a magnified image (zoom-in) of the surface and (e) line, histogram as x and y graph.

Copyright © 2021 *Al-Mustansiriyah Journal of Science*. This work is licensed under a Creative Commons Attribution Noncommercial 4.0 International License.

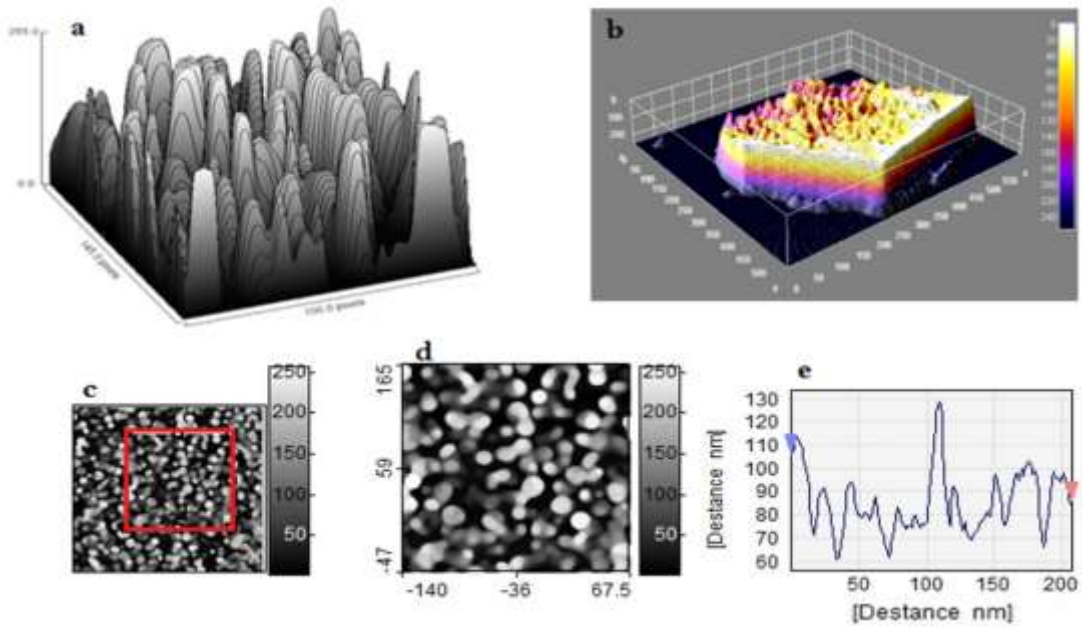

Figure 7. (a and b) Represent a 3D image of SnO_2 thin films doped with 8 wt % of Cu, (c) 2D image, (d) a magnified image (zoom-in) of the surface and (e) line, histogram as x and y graph.

OPTICAL PROPERTIES

Figure (8-a) explains the transmittance spectrum of SnO_2 thin films doped with a different weight ratio of copper (0, 2, 4, 6, 8) wt%. Further, the lowest transmittance percentage was for copper at (6 and 8) wt%, while the highest value of transmittance for (0 and 2) wt%. increasing distortion near the grain border, which contributed to the scattering of the incident light. In addition, to the occurrence of displacement in the edge of absorption towards the longer wavelengths, or in other words towards the lower energy gap with the increase in the doping weight ratio wt%, this can be explained within the quantum confinement.

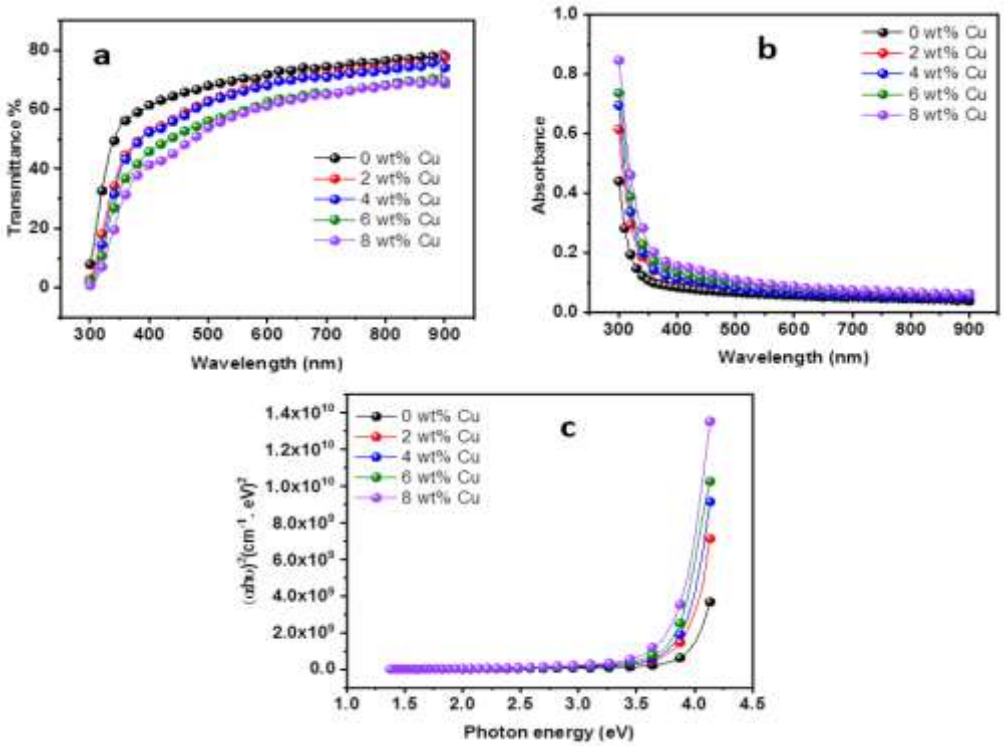

Figure 8. illustrated (a) the transmittance spectrum (b) the absorbance spectrum and (b) $(\alpha h\upsilon)^2$ as function to hυ, of SnO_2 thin films doped with a different weight ratio of copper (0, 2, 4, 6, 8) wt%.

In the figure (8-b), the absorption spectrum of SnO_2 thin films doped with a different weight ratio of copper (0, 2, 4, 6, 8) wt%, prepared by RF reactive magnetron sputter. It is noted the highest absorption value was for the model with a weight ratio of copper 8 wt%. Due to the entry of impurity of copper atoms within the crystal structure of SnO_2, led to formation of localized levels within the energy E_g. In addition, it is noted that absorbance values decrease with decreasing wavelength.

The reason is the incident photon could not excite the electrons in valence band V.B. and raise them to the conduction band C.B. due to the large E_g compared to the energy of the incident photon.

The figure (8-c) represents the $E_g^{Op.}$ of SnO_2 thin films doped with a different weight ratio of copper (2, 4, 6, 8) wt%. The $E_g^{Op.}$ values has been calculated from the relation (4) by plotting a graph relation between $(\alpha h\upsilon)^2$ and photon energy $h\upsilon$ [31]. Then, from the extend the straight part of the curve that cuts the X-axis that represents the energy gap at point $(\alpha h\upsilon)^2 = 0$, which is equal to $E_g^{Op.}$. In addition, it is noted the $E_g^{Op.}$ decrease with increasing doped copper. The reason is due to the improvement of crystallization for the weight ratio of copper (6 and 8) wt% with the appearance of localized levels to the forbidden $E_g^{Op.}$ that reduces the energy needed to transfer the electron from V.B to C.B.

$$h\vartheta = B(h\vartheta - E_g^{op.})^r \qquad (4)$$

Where α represents the optical absorbance coefficient (cm^{-1}), B is a constant, and r is a transition order.

CONDUCTIVITY PERFORMS

Figure (9-a), the optical conductivity of pure and Cu doped SnO_2 in weight ratio (2, 4, 6 and 8) wt%, as a function of the photon energy eV, where the optical conductivity was calculated from the equation (5).

We can calculate the optical conductivity $\sigma_{Op.}$through the electric field accompanying the falling electromagnetic wave (UV and vis) by applying the Drude band model. Where it represents E and w the electric field and the angular frequency of the electromagnetic wave in respectively, and τ is a frequency of collisions between electrons and the lattice atoms.

$$\sigma_{Op.} = \frac{ne}{\tau}\left[\!\left[\frac{eE}{mw\left(wt+\frac{1}{\tau}\right)}\right]\!\right] \qquad (5)$$

Where $\sigma_{Op.}$ The optical conductivity, E is electric field, n as number of electrons, $\frac{1}{\tau}$ collision frequency, e the electron charge, m is electron mass, and w as incident light frequency. Since we are dealing with high frequencies $w \gg \frac{1}{\tau}$, we get,

$$\sigma_{Op.} = \frac{ne^2}{m\tau w^2} \qquad (6)$$

The optical conductivity $\sigma_{Op.}$, decrease from 3.88 eV to 2.87 eV with the increase in doping weight ratio from 2 wt% to 8 wt%; Due to that all electrons under 3.88 eV are confined by their holes in the V.B.

Therefore, there is no current from the pair (e-h) and as the energy of the falling photon increases, the electrons continue to excite generated charge carriers and the optical current is generated.

Where c is light speed and n_o is the refractive index.

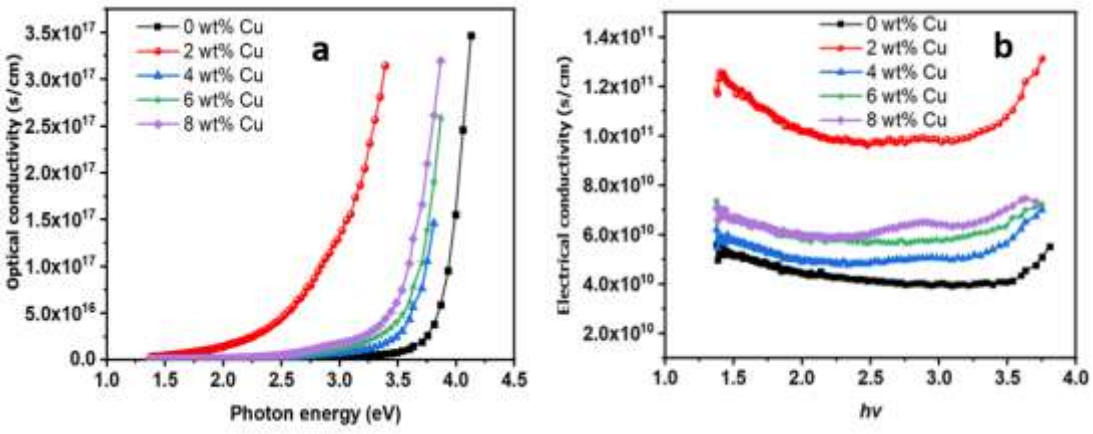

Figure 9. shown (a) the optical conductivity and (b) the electrical conductivity of SnO_2 thin films doped with a different weight ratio of copper (0, 2, 4, 6, 8) wt%.

Copyright © 2021 *Al-Mustansiriyah Journal of Science*. This work is licensed under a Creative Commons Attribution Noncommercial 4.0 International License.

Figure (9-b) represents the relationship between electrical conductivity $\sigma_{Ele.}$ and photon energy for pure and Cu doped SnO_2 thin films. It is noted from the figure that the highest conductivity was 3.72 eV and 3.63 for the two doping weight ratios (2 and 8) wt% respectively.

Where these values were obtained from the equation (6) the comparison between the optical conductivity and the electrical conductivity figure (11 and 12) and as it is listed in Table (2) we note that the behavior are similar and in turn similar to behavioral energy gap behavior.

$$\sigma_{Ele.} = \frac{2\lambda\sigma_{OP.}}{\alpha} \qquad (7)$$

Where: λ is the wavelength of the incident photon, and α is the absorption coefficient.

Table (2) Comparison between the electrical and optical conductivity

Doping ratio wt%	Electrical con. eV	Optical con. eV
0	3.805	3.880
2	3.740	2.870
4	3.750	3.610
6	3.750	3.630
8	3.630	3.500

CONCLUSIONS

The films were prepared doped and undoped with different copper weight ratios, and showed a poly-crystalline diffraction pattern. Moreover, there is no reflection of copper even with the highest percentage of deformation according to the international card JCPOS No. 41-1445. The intensity of the predominant reflection (110) increases with the distortion, especially the copper weight ratio (6 and 8) wt%. Consequently, the improvement crystallization led to a decrease in the values of the $E_g^{Op.}$, and that the transitions are direct transitions allowed. In addition to the high convergence in the electrical and optical conductivity values that are calculated from the optical transmittance values, it increases the deformation with copper nanoparticles weight ratio.

ACKNOWLEDGMENT

Authors would like to extend their thanks and gratitude to the department of physics at the college of science of the Mustansiriyah University, Tray loge, and advanced material Lab. We wish also to acknowledge the department of physics staff at the college of education at Mustansiriyah University.

REFERENCES

[1] O. Abdulmunem, K. Hassoon, M. Gaafar, A. Rahimi-Iman, and J. C. Balzer, "TiN Nanoparticles for Enhanced THz Generation in TDS Systems," *J. Infrared, Millimeter, Terahertz Waves*, vol. 38, no. 10, pp. 1206–1214, 2017, doi: 10.1007/s10762-017-0412-z.

[2] Mohammed Ali Mohammed Jassim, J. M. Chauveau, and T. Bretagnon, "Time-resolved photoluminescence investigation of (Mg, Zn) O alloy growth on a non-polar plane," *Superlattices Microstruct.*, 2018, doi: 10.1016/j.spmi.2018.02.001.

[3] S. J. Mezher, K. J. Kadhim, O. M. Abdulmunem, and M. K. Mejbel, "Microwave properties of Mg–Zn ferrite deposited by the thermal evaporation technique," *Vacuum*, vol. 173, p. 109114, Mar. 2020, doi: 10.1016/j.vacuum.2019.109114.

[4] A. K. H. Albarazanchi, A. Al-Haddad, and M. F. Sultan, "Plasmonic Enhancement Mechanism of Template-Based Synthesized Au@TiO_2 Nanodiscs," *ChemNanoMat*, vol. 7, no. 1, pp. 27–33, Jan. 2021, doi: 10.1002/cnma.202000513.

[5] C. A. Hoel, T. O. Mason, J. F. Gaillard, and K. R. Poeppelmeier, "Transparent conducting oxides in the ZnO-In_2O_3-SnO_2 system," *Chem. Mater.*, vol. 22, no. 12, pp. 3569–3579, 2010, doi: 10.1021/cm1004592.

[6] T. Minami, "Transparent conducting oxide semiconductors for transparent electrodes," *Semicond. Sci. Technol.*, vol. 20, no. 4, 2005, doi: 10.1088/0268-1242/20/4/004.

[7] E. Elangovan, M. P. Singh, M. S. Dharmaprakash, and K. Ramamurthi, "Some physical properties of spray deposited SnO_2 thin films," *J. Optoelectron. Adv. Mater.*, vol. 6, no. 1, pp. 197–203, 2004.

[8] E. S. Hassan, A. N. Abd, and M. O. Dawood, "The Sputter Time Duration Effect on the Structural and Optical Properties of Zinc Oxide by RF Magnetron Sputtering," *Silicon*, vol. 10, no. 6, pp. 2901–2906, 2018, doi: 10.1007/s12633-018-9831-2.

[9] J. C. Manifacier, M. De Murcia, J. P. Fillard, and E. Vicario, "Optical and electrical properties of SnO2 thin films in relation to their stoichiometric deviation and their crystalline structure," *Thin Solid Films*, vol. 41, no. 2, pp. 127–135, 1977, doi: 10.1016/0040-6090(77)90395-9.

[10] M. M. Bagheri-Mohagheghi and M. Shokooh-Saremi, "The influence of Al doping on the electrical, optical and structural properties of SnO2 transparent conducting films deposited by the spray pyrolysis technique," *J. Phys. D. Appl. Phys.*, vol. 37, no. 8, pp. 1248–1253, 2004, doi: 10.1088/0022-3727/37/8/014.

[11] A. F. Khan, M. Mehmood, A. M. Rana, and M. T. Bhatti, "Effect of annealing on electrical resistivity of

rf-magnetron sputtered nanostructured SnO 2 thin films," *Appl. Surf. Sci.*, vol. 255, no. 20, pp. 8562–8565, 2009, doi: 10.1016/j.apsusc.2009.06.020.

[12] A. J. Galdikas *et al.*, "Peculiarities of surface doping with Cu in SnO_2 thin film gas sensors," *Sensors Actuators, B Chem.*, vol. 43, no. 1–3, pp. 140–146, 1997, doi: 10.1016/S0925-4005(97)00206-2.

[13] S. M. A. Durrani, "Biasing voltage dependence of sensitivity of electron beam evaporated SnO2 thin film CO sensor," *Sensors*, vol. 6, no. 9, pp. 1153–1160, 2006, doi: 10.3390/s6091153.

[14] B. K. Min and S. D. Choi, "SnO_2 thin film gas sensor fabricated by ion beam deposition," *Sensors Actuators, B Chem.*, vol. 98, no. 2–3, pp. 239–246, 2004, doi: 10.1016/j.snb.2003.10.023.

[15] S. Shukla, V. Venkatachalapathy, and S. Seal, "Thermal Evaporation Processing of Nano and Submicron Tin Oxide Rods," *J. Phys. Chem. B*, vol. 110, no. 23, pp. 11210–11216, Jun. 2006, doi: 10.1021/jp061009b.

[16] S. S. Chiad, H. A. Noor, O. M. Abdulmunem, and N. F. Habubi, "Optical and structural properties of Ni-doped Co_3O_4 Nanostructure thin films via CSPM," *J. Phys. Conf. Ser.*, vol. 1362, no. 1, 2019, doi: 10.1088/1742-6596/1362/1/012115.

[17] D. G. Rickerby and A. M. Serventi, *Nanostructured Metal Oxide gas sensors for air-quality monitoring*, 1st ed. Elsevier, 2010.

[18] S. Tarish *et al.*, "Highly efficient biosensors by using well-ordered ZnO/ZnS core/shell nanotube arrays," *Nanotechnology*, vol. 28, no. 40, p. 405501, Oct. 2017, doi: 10.1088/1361-6528/aa82b0.

[19] R. Brahma, M. G. Krishna, and A. K. Bhatnagar, "Optical, structural and electrical properties of Mn doped tin oxide thin films," *Bull. Mater. Sci.*, vol. 29, no. 3, pp. 317–322, 2006, doi: 10.1007/BF02706503.

[20] R. A. Afre, N. Sharma, M. Sharon, and M. Sharon, "Transparent conducting oxide films for various applications: A review," *Rev. Adv. Mater. Sci.*, vol. 53, no. 1, pp. 79–89, 2018, doi: 10.1515/rams-2018-0006.

[21] P. Chetri, B. Saikia, and A. Choudhury, "Structural and optical properties of Cu doped SnO_2 nanoparticles: An experimental and density functional study," *J. Appl. Phys.*, vol. 113, no. 23, 2013, doi: 10.1063/1.4811374.

[22] M. Batzill and U. Diebold, "The surface and materials science of tin oxide," *Prog. Surf. Sci.*, vol. 79, no. 2–4, pp. 47–154, 2005, doi: 10.1016/j.progsurf.2005.09.002.

[23] M. M. Bagheri-Mohagheghi and M. Shokooh-Saremi, "Investigations on the physical properties of the SnO2-ZnO transparent conducting binary-binary system deposited by spray pyrolysis technique," *Thin Solid Films*, vol. 441, no. 1–2, pp. 238–242, 2003, doi: 10.1016/S0040-6090(03)00948-9.

[24] A. K. and C. C. Holliday, "Modern Inorganic Chemistry," 1975, [Online]. Available: https://www.amazon.com/Modern-Inorganic-Chemistry-Kenneth-Holliday/dp/0408706635.

[25] S. J. Mezher, M. O. Dawood, O. M. Abdulmunem, and M. K. Mejbel, "Copper doped nickel oxide gas sensor," *Vacuum*, vol. 172, p. 109074, 2020, doi: 10.1016/j.vacuum.2019.109074.

[26] R. Li *et al.*, "Influence of Charge Carriers Concentration and Mobility on the Gas Sensing Behavior of Tin Dioxide Thin Films," *Coatings*, vol. 9, no. 9, p. 591, 2019, doi: 10.3390/coatings9090591.

[27] J. A. M. C.Robert, Weast, "CRC Handbook of Chemistry and Physics: A Ready-Reference of Chemical and Physical Data," *J. Am. Chem. Soc.*, vol. 127, no. 12, pp. 4542–4542, Mar. 2005, doi: 10.1021/ja041017a.

[28] T. W. Kim, D. U. Lee, J. H. Lee, D. C. Choo, M. Jung, and Y. S. Yoon, "Structural, electrical, and optical properties of SnO_2 nanocrystalline thin films grown on p-InSb (111) substrates," *J. Appl. Phys.*, vol. 90, no. 1, pp. 175–180, 2001, doi: 10.1063/1.1372159.

[29] "[dataset] Joint Committee on Powder Diffraction Standards (JCPDS), International Centre for Diffraction Data, Card No. 41-1445," 1997. [Online]. Available: http://id.loc.gov/authorities/names/n78034812. http://www.mathijs.be/01h8dg/kgl58g.php?pdl=jcpds-card-pdf.

[30] E. S. Hassan, A. K. Elttayef, S. H. Mostafa, M. H. Salim, and S. S. Chiad, "Silver oxides nanoparticles in gas sensor applications," *J. Mater. Sci. Mater. Electron.*, vol. 30, no. 17, pp. 15943–15951, 2019, doi: 10.1007/s10854-019-01954-1.

[31] E. S. Hassan *et al.*, "Structural, Morphological and Optical Characterization of Tin Doped Zinc Oxide Thin Film by (SPT)," *J. Phys. Conf. Ser.*, vol. 1234, no. 1, 2019, doi: 10.1088/1742-6596/1234/1/012013.

Copyright © 2021 *Al-Mustansiriyah Journal of Science*. This work is licensed under a Creative Commons Attribution Noncommercial 4.0 International License.